Journal of Zhejiang University-SCIENCE C (Computers & Electronics)
ISSN 1869-1951 (Print); ISSN 1869-196X (Online)
www.zju.edu.cn/jzus; www.springerlink.com
E-mail: jzus@zju.edu.cn

Studying pressure sores through illuminant invariant assessment of digital color images

Sahar MOGHIMI[†1], Mohammad Hossein MIRAN BAYGI[†‡1], Giti TORKAMAN[2], Ehsanollah KABIR[1], Ali MAHLOOJIFAR[1], Narges ARMANFARD[1]

([1]*Department of Electrical Engineering, Tarbiat Modares University, P.O. Box 14115-111, Tehran, Iran*)

([2]*Department of Physical Therapy, Tarbiat Modares University, P.O. Box 14115-111, Tehran, Iran*)

[†]E-mail: {moghimi, miranbmh}@modares.ac.ir

Received Sept. 7, 2009; Revision accepted Jan. 29, 2010; Crosschecked July 1, 2010

Abstract: Methods for pressure sore monitoring remain both a clinical and research challenge. Improved methodologies could assist physicians in developing prompt and effective pressure sore interventions. In this paper a technique is introduced for the assessment of pressure sores in guinea pigs, using captured color images. Sores were artificially induced, utilizing a system particularly developed for this purpose. Digital images were obtained from the suspicious region in days 3 and 7 post-pressure sore generation. Different segments of the color images were divided and labeled into three classes, based on their severity status. For quantitative analysis, a color based texture model, which is invariant against monotonic changes in illumination, is proposed. The texture model has been developed based on the local binary pattern operator. Tissue segments were classified, using the texture model and its features as inputs to a combination of neural networks. Our method is capable of discriminating tissue segments in different stages of pressure sore generation, and therefore can be a feasible tool for the early assessment of pressure sores.

Key words: Local binary pattern (LBP), Automatic assessment, Neural networks, Color based texture model, Pressure sores, Digital color images

doi:10.1631/jzus.C0910552 **Document code:** A **CLC number:** TP391

1 Introduction

Pressure sores occur when an unrelieved pressure causes ischemia, which, if prolonged, can lead to the development of necrotic tissue (Salcido *et al*., 1995). Pressure sores are notably different from acute wounds in that, unlike acute wounds, they can develop both superficially and/or from within the deep tissue, depending on the nature of the surface loading (Bader *et al*., 2005). Pressure sores are a major problem for patients with impaired mobility and reduced ability to sense injury. Therefore, daily checks are required in at-risk patients for signs of erythema or redness which may indicate the generation of pressure sores.

Different imaging techniques, such as digital photography, high frequency ultrasound, computerized tomography (CT), and magnetic resonance imaging (MRI), can be used for the early assessment of pressure sores. CT and MRI are not economical and cannot be employed in small offices and/or clinics. In addition, CT and MRI have the concerns of exposure to X-rays, injected dyes, magnetic fields, and also a practical delay in final report generation. High frequency ultrasound does not have the above problems, but it is rather expensive and the training is intensive as well as user-dependent. Digital photography has been widely used for the assessment of wounds and pressure ulcers (Belem, 2004; Salter *et al*., 2006; Treuillet *et al*., 2009). Although this technique does not provide information about the underlying tissue, its low cost and ease of use and interpretation have made it a desirable tool for the as-

‡ Corresponding author

sessment of pressure sores. Also, different image processing techniques have been developed to provide quantitative interpretation tools for studying the captured images.

Changes in the color content of digital photographs have demonstrated to provide a viable tool for assessment of wounds in general. Hansen *et al.* (1997) used color images to score artificially-induced pressure sores in animals based on changes in the hue component. Herbin *et al.* (1993) used color images of the wound surface to extract the area and a color index for monitoring tissue changes during wound healing. Berriss and Sangwine (1997) used three-dimensional (3D) RGB histograms for clustering different tissue types in the pressure ulcer bed. Several researchers tried to cluster or segment wound images using different sets of features including textural features as well as those extracted from RGB, HSV, HIS, LAB, and LUV histograms (Jones and Plassmann, 1995; Berriss and Sangwine, 1997; Nischik and Forster, 1997; Bon *et al.*, 2000; Perez *et al.*, 2001; Belem, 2004; Zheng *et al.*, 2004; Galushka *et al.*, 2005; Kolesnik and Fexa, 2005). Bon *et al.* (2000) used color content of captured images to define a healing curve for the assessment of wound healing. Another research team used an adaptive spline technique to segment the wound boundary in the images of venous leg ulcers based on hue, saturation, and intensity measures (Oduncu *et al.*, 2004). Although color features have proven to be useful for the segmentation of wound tissue and assessment of healing, their values are dependent on the effect of surrounding light and specifications of the image capturing system (Plassmann *et al.*, 1995; Plassmann and Jones, 1998; Malian *et al.*, 2005). Therefore, precautions should be taken in image acquisition. Comparison of wound status in different time intervals is not reliable unless images are obtained under the same surrounding light conditions, or a color calibration phase is included in the preprocessing steps. Researchers have exercised different color calibration techniques to address the above issue (Diao *et al*., 2005; Bianco *et al.*, 2007; Lee and Choi, 2008).

In this paper, we introduce a technique for studying pressure sore generation from the color content of captured images, regardless of the surrounding light. It is illustrated that as color changes are measured with respect to the adjacent healthy tissue, no precaution has to be considered about the surrounding light. In fact, we have shown that the introduced model is invariant against monotonic color variations across the image. For evaluating the efficiency of the proposed model, different segments of the captured images are labeled, based on their severity status, and classified using the proposed model and a combination of neural networks.

2 Materials and methods

2.1 Pressure sore generation

2.1.1 Animals

We used six healthy male albino guinea pigs (Dunkin-Hartley; Pasteur Institute of Iran, Tehran, Iran) that were 4 to 6 months old and weighed 400 to 450 g. The animals were maintained in special cages under controlled conditions according to the experimental guidelines of Tarbiat Modares University. Up to 12 h before the anesthesia and pressure application, the animals had unlimited access to food. The Ethics Commission of Tarbiat Modares University approved the study.

2.1.2 Procedure

After weighing the animals, we prepared the anesthesia using a mixture of xylazine (20 mg/ml) and ketamine hydrochloride (Brown *et al.*, 1995) (100 mg/ml; 1 to 8 cc, injection of 1 cc/kg).

The system for generation of pressure sores included a PWM (pulse width modulation) card (Control of Biological Systems LAB, Amir Kabir University, Tehran, Iran), an A/D (analog to digital) card, a PC, a mechanical arm, and two 12 V DC motors (MicroMo, USA). The rotational output of the motors was converted to a linearly driven indentor, using a mechanical interface. Two strain gauges (HBM, Germany) were assembled on a small horizontal arm facing each other to measure the applied force. The sensor signal was linearized after passing through the A/D card. A/D output provided the control signal. A PID (proportional-integral-derivative) controller (Control of Biological Systems LAB, Amir Kabir University, Tehran, Iran) was used to keep the difference between the desired and applied loads as

small as possible. The user was able to monitor the applied pressure throughout the wound generation sessions for the duration of the experiment. A block diagram of the system is illustrated in Fig. 1. The ability of the system to produce pressure sores was previously tested based on histological analysis (Torkaman *et al.*, 2000). A photograph of the system used for generating pressure sores is shown in Fig. 2.

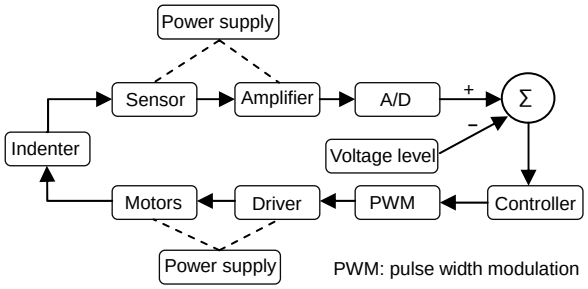

Fig. 1 Block diagram of the pressure sores generation system

Fig. 2 The setup used for generating pressure sores

Pressure was uniformly applied to a disk of diameter 0.75 cm. The load was kept constant at (400±5) g for 5 h over the trochanter region of the right animal hind limb.

2.2 Data preparation

Digital images were obtained from the region of interest (ROI) in days 3 and 7 post-pressure sore generation using a 7-megapixel Canon digital camera in normal day light in the laboratory without any internal illumination. The reason for choosing these days for tissue monitoring is that the pressure sore, induced in this manner, reaches its maximum severity after seven days (Daniel *et al.*, 1981; Torkaman *et al.*, 2000), and the full extent of tissue damage is not apparent until the fifth through the seventh day. It has also been stated that before this time, the actual extent of deep necrosis is difficult to define and after that healing reverses some of the more obvious signs of damage (Hansen *et al.*, 1997). By monitoring the tissue in the above days, we were more certain that we were assessing pressure sore generation. The ROI was marked on the sample's skin. The animals were kept in a restrainer during image acquisition sessions to provide more accurate images and avoid motion artifacts. The size of the captured images was reduced to 480×480 pixels with the suspicious region at the center of the image. Every 40×40-pixel segment of the RGB images was labeled by three physicians. Each physician was asked to classify every region into one of three different classes, with I, II, and III referring to intact, slightly damaged, and considerably damaged tissues respectively. The label of the class corresponding to the highest number of physician votes was considered as the final label of the region under study. Table 1 illustrates the results of labeling different regions (segments) into the above three classes.

The RGB color images were converted to the HSV color space, and the hue component was considered for further processing steps. This allowed us to develop our model based on the color content of the captured images. The hue component values were normalized to take values in the interval [0, 1].

Table 1 Number of segments in each class

Class	Description	Number of members
I	Intact	1552
II	Slightly damaged	137
III	Considerably damaged	39

2.3 Modeling the color content

We utilized texture information when modeling the color content of each segment. The local binary pattern (LBP) texture operator was selected as the measure of texture because it is invariant with respect to the monotonic grayscale changes (Ojala *et al.*, 1996; Heikkila and Pietikainen, 2006). This operator has shown an excellent performance in different applications (Haralick *et al.*, 1973; Ahonen *et al.*, 2006; Heikkila and Pietikainen, 2006; Armanfard *et al.*, 2008; Mackiewicz *et al.*, 2008; Tajeripour *et al.*, 2008).

The LBP operator labels the pixels of an image

region by thresholding the values of neighborhood pixels with respect to the central pixel. After the threshold is set, the values of the pixels in the neighborhood produced are multiplied by the binomial weights given to the corresponding pixel. The values of the pixels (in the predefined neighborhood) are summed together to obtain the LBP number of the central pixel. To make the LBP invariant to the small color changes, i.e., the presence of hair roots in the ROI, the outcome of thresholding was considered to be one, only if the difference between the neighbor and the central pixel was larger than t (defined threshold). The smaller was the value of t, the smaller were the changes in tissue color allowed to affect the outcome of the thresholding process. For calculating this value the hue component of an image obtained from the wound tissue was taken into account. Different threshold values were tested in ascending order until the LBP values of the intact regions became very small with respect to the LBP values of the wound tissue. Fig. 3 shows the LBP values of the pixels obtained using different threshold values. For visual interpretation these values are illustrated as grayscale images. While higher values of t cause meaningful changes in hue values to be undetectable, for very smaller values of t the LBP operator detects undesirable changes in the hue values due to the presence of hair roots.

The LBP operator is formulated as

$$b_i = \begin{cases} 1, & I(x_i, y_i) - I(x_0, y_0) > t, \\ 0, & I(x_i, y_i) - I(x_0, y_0) \le t, \end{cases} \tag{1}$$

$$\mathrm{LBP}(x_0, y_0) = \sum_{i=0}^{N-1} b_i 2^i, \tag{2}$$

where $I(x_i, y_i)$ is the value of the pixel location (x_i, y_i) in the neighborhood, i=0, 1, …, N−1. The value of i increases in a counter clockwise manner starting from the top left corner of the neighborhood. The process discussed above is illustrated in Fig. 4. Note that different neighborhood sizes may be adopted for calculating the LBP values. Based on our previous experiments the value of t was set to 0.05.

The texture model for a pixel developed in this research consisted of its LBP value, computed over a defined region around that pixel (a 3×3 pixel neighborhood). In the first attempt, the LBP histogram of each segment was used as its feature vector. We applied this operator to the hue channel of the HSV space for detecting changes in the tissue color. The model of every 40×40 region of the 480×480 images was generated as mentioned above. To reduce the processing time, in the next step, the original LBP histograms were replaced by three features extracted

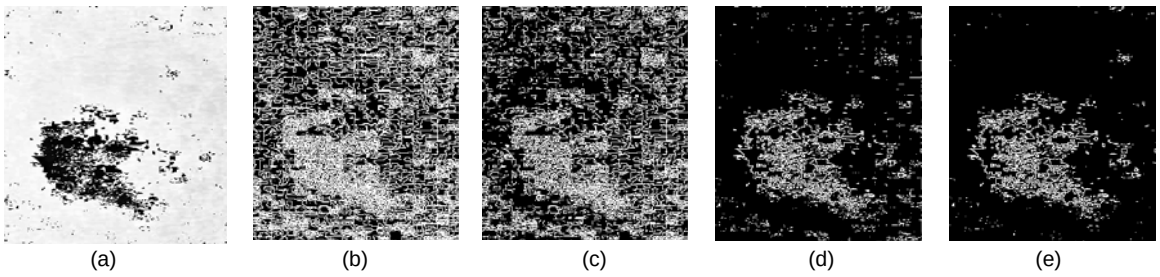

Fig. 3 (a) The hue component of a wound image. Local binary pattern (LBP) values of (a), calculated for different threshold values and illustrated as grayscale images: t=0.01 (b), t=0.02 (c), t=0.04 (d), and t=0.05 (e)

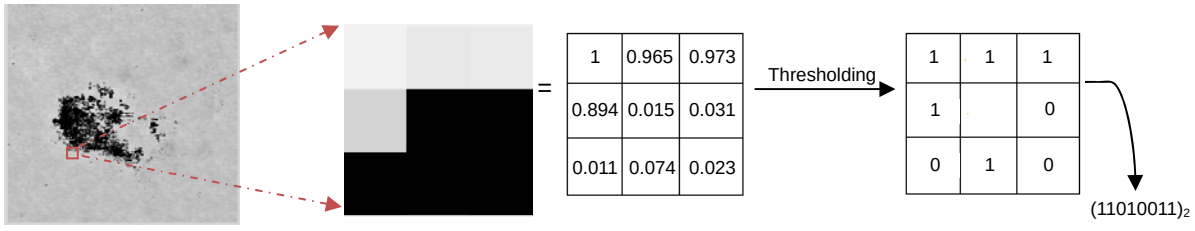

Fig. 4 An example for calculating the local binary pattern (LBP) values
From left to right: the hue component, the magnified hues and their values, and the threshold binary values

from them. The extracted features were their entropy, variance, and kurtosis (Theodoridis and Koutroumbas, 2003).

Entropy:

$$H = -\sum_{I=0}^{N_g-1} P(I)\log_2 P(I). \quad (3)$$

Variance:

$$\mu_2 = \sum_{I=0}^{N_g-1} (I-m)^2 P(I). \quad (4)$$

Kurtosis:

$$\mu_4 = \sum_{I=0}^{N_g-1} (I-m)^4 P(I). \quad (5)$$

Herein N_g is the total number of possible LBP values. $P(I)$ and m represent the probability of the presence of I and the mean LBP value in the neighborhood, respectively. Both ideas (original LBP histogram and the extracted features) were tested for their capabilities to discriminate segments belonging to different classes introduced earlier.

2.4 Classification

We tried to classify the labeled segments based on the features extracted from the texture model. Multi-layered perceptron neural networks (MLP NNs) were used to classify the segments into the three different classes. Three networks with similar structures were used. Each network was trained to discriminate one specific class from the others. All nodes had a tan-sigmoid transfer function. The weights and biases of the networks were initialized with random values, taken from −1 to 1. We used batch training where the weights between the neurons are updated only after all the training examples are exposed to the network. We also used Levenberg-Marquardt back-propagation for training and found that, in practice, this method produced the best result. For the classification of segments using the LBP histograms, the networks had 256 input neurons and 2 hidden layers with 20 and 7 neurons respectively. For classifying the histogram features, a network with 3 input neurons and 1 hidden layer (with 8 neurons) produced the best result. Note that the number of hidden layers as well as their neurons was chosen based on the experiments we conducted.

Due to the small number of samples in two of our classes (classes II and III) and the dimensions of the feature vectors, we used 5-fold cross-validation to avoid any bias or error during segment classification.

Since three neural networks were trained on the data, the outputs of the networks had to be combined to obtain the final decision. The final decision (D) was produced as $D=i$, if $d_i=\max(d_1, d_2, d_3)$, where i=1, 2, or 3 and d_1, d_2, and d_3 were the decisions of the three classifiers. This means that a class label was assigned as the final decision, if the soft decision of the network trained on the samples of that specific class was higher than those of the other two networks. In fact d_i was the probability of assigning a feature vector to class i by the ith classifier.

3 Results and discussions

Fig. 5 shows two RGB color images obtained from the same guinea pig in days 3 and 7 post-pressure sore generation. Figs. 5b and 5c illustrate the polar histogram of the hue of these segments. Although both digital color images (Figs. 5a and 5f) were captured from the same animal, the hue shift was noticeable in the transition from polar histograms Figs. 5b and 5c to polar histograms Figs. 5g and 5h. The reason for this artifact is that no precautions were taken about the light conditions. On the other hand, the peaks of the four LBP histograms (Figs. 5d, 5e, 5i, and 5j), calculated over the hue component, happened to occur at the same location (at zero). This phenomenon has a simple analytic meaning. Since the monotonic color shift can be expressed as a constant offset (os) in the hue value of each pixel, the left term of the condition in Eq. (1) under monotonic color shift becomes ($I(x_i, y_i)-\text{os})-(I(x_0, y_0)-\text{os})$, which is exactly the same as $I(x_i, y_i)-I(x_0, y_0)$. This illustrates that the LBP histogram is invariant against monotonic color shifts from one day to another, and therefore is a reliable tool for comparing the color images, obtained under monotonically variant illumination.

Fig. 6 shows the LBP histograms of the three different segments, each belonging to one of the classes under study. The value of the histograms at zero was omitted for illustration purposes. The histograms were normalized by dividing their values to

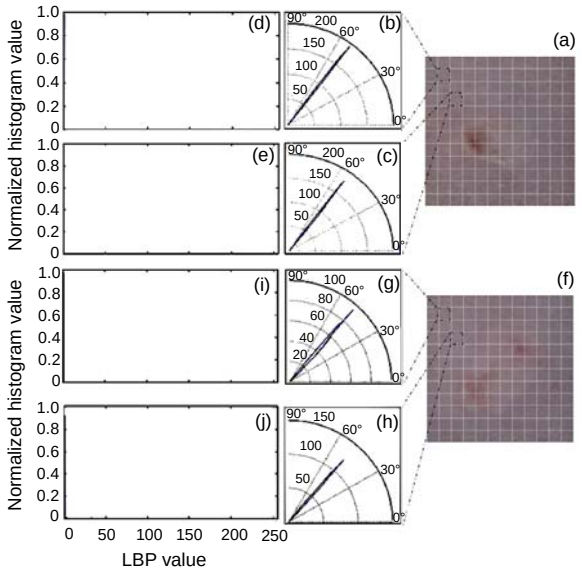

Fig. 5 Wound images and their hue and local binary pattern (LBP) histograms

(a) is the RGB color image obtained from one animal on day 7. (b) and (c) are polar histograms of hue computed for the dashed squares of (a). (d) and (e) are LBP histograms of the same regions used in (b) and (c). (f) is the RGB color image obtained from the same animal on day 3. (g) and (h) are polar histograms of hue computed for the dashed squares of (f). (i) and (j) are LBP histograms of the same regions used in (g) and (h). The dashed squares in (a) and (f) represent two healthy segments of tissue on days 7 and 3, respectively

the number of pixels in each segment. It is obvious that the LBP histogram of a healthy segment had a very small value at locations other than zero. This is because the color content of a healthy segment has a homogeneous pattern. Pressure sore generation causes inhomogeneities in the color content, as a result of the appearance of skin redness and erythema. As the pressure sore reaches more severe stages, or in other words progresses to superficial layers, color inhomogeneities become significant, resulting in a rough histogram. An LBP histogram of a segment that belongs to class III is presented in Fig. 6c. The threshold value introduced in Eq. (1) plays an important role in detecting the color differences. Therefore, the sensitivity of the model in the assessment of pressure sore generation is highly related to this threshold value.

Fig. 6 shows the difference between the three observation classes heuristically. It is desirable to know whether the features extracted from the LBP histogram have the ability to discriminate the segments that illustrate different stages of pressure sore generation. Table 2 shows the significance of extracted features examined by analysis of variance and multiple comparisons. Based on the confidence interval, and that the interval does not include zero, the mean of these three classes are considerably different and there is a meaningful difference between the three classes under study. Therefore, it may be concluded that the extracted features are able to discriminate the samples belonging to different classes, and are good candidates for the purpose of classification. The box-plots of the extracted features are presented in Fig. 7, for providing a better comprehension about the class separability. On each box, the central mark is the median. The edges of the box are the 25th and 75th percentiles. The whiskers extend to the most extreme data points, outliers not considered. The outliers are plotted individually.

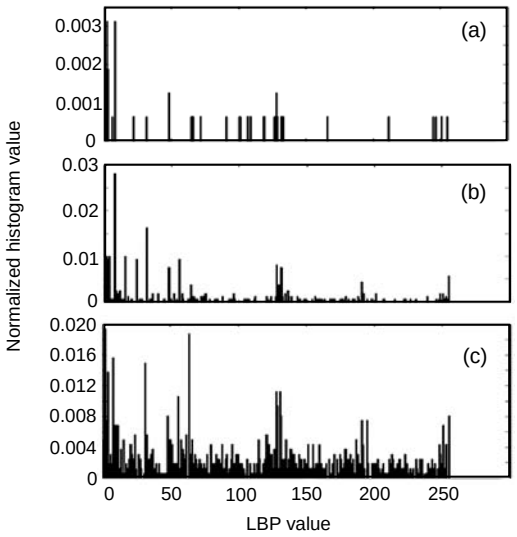

Fig. 6 Local binary pattern (LBP) histograms of hue segments belonging to classes I (a), II (b), and III (c)

The value of the histograms at zero is omitted for illustration purposes

Table 3 shows the classification results over the test samples, using two different feature vectors, namely LBP histograms and its features. As one would predict, feeding the entire LBP histogram into the classifiers results in greater accuracy. The highest percentage of misclassified samples belongs to class II. This was expected, since this class includes the

Table 2 Class separability studied through one way analysis of variance and multiple comparisons

Class	MD (95% CI)		
	Entropy	Variance	Kurtosis
I/II	−0.3799 [−0.4036, −0.3562]	0.0103 [0.0098, 0.0108]	0.9972 [0.8947, 1.0997]
I/III	−0.9904 [−1.0335, −0.9473]	0.0289 [0.0279, 0.0298]	3.3084 [3.1220, 3.4948]
II/III	−0.6105 [−0.6588, −0.5622]	0.0186 [0.0175, 0.0196]	2.3112 [2.1025, 2.5199]

MD: mean difference; CI: confidence interval

Table 3 Classification results

Input	Total accuracy (%)	Training time (min)	Percentage of misclassified samples (%)		
			Class I*	Class II**	Class III***
LBP histogram	97.97	420	0. 32	19	0.00
LBP features	95.94	1.5	0. 67	38	0.00

* n=311; ** n=26; *** n=9. n is the number of samples in each class

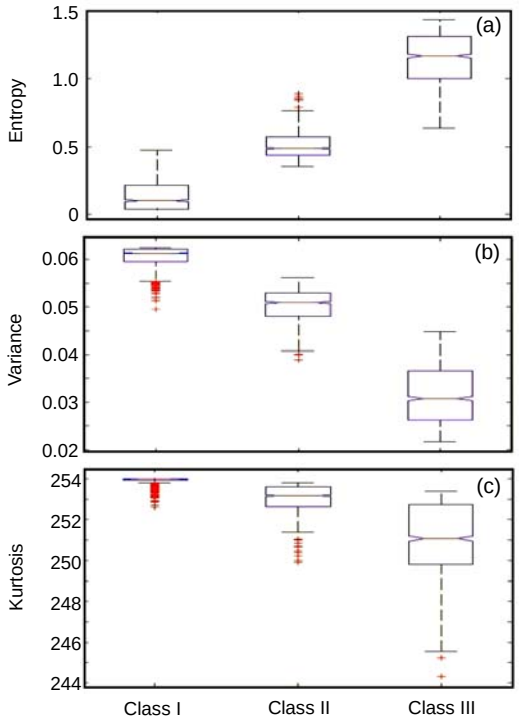

Fig. 7 Box-plots of the extracted feature
(a) Entropy; (b) Variance; (c) Kurtosis. These values are plotted for all the samples (including test and training)

segments that were only slightly damaged. Therefore, tissue segments with faint erythema or redness can be misinterpreted as intact tissue.

As the pressure sores were induced in guinea pigs, the hypothesis could not be tested on more severe sores due to ethical considerations.

The number of segments belonging to class III was very small compared with that of class I. This was due to the small dimension of the pressure disk used for inducing the sores. The size of the pressure applicator disk was chosen based on the size of the animal trochanter. We could not reduce the image dimension either, as it was necessary to monitor the adjacent tissue for tracking the pressure sores. Increasing the number of images would not help, as the ratio of samples in class III to the samples in class I would still be small. Nevertheless, the test samples belonging to class III, with the smallest numbers, were still classified with high accuracy.

The number of segments labeled into class III by the clinicians was higher in the images of day 7 than in the images of day 3. This implies that the images of day 7 illustrated more severe stages of pressure sores. Therefore, different captured images may also be compared based on the pressure sore severity by counting the number of segments classified into the three mentioned classes. This would provide a relative measure for monitoring the pressure sore generation. Bon *et al*. (2000) also introduced a relative measure of wound healing, but it was based on the changes in the RGB components. Herbin *et al*. (1993) used a color index for monitoring healing but they provided their image database with precautions about surrounding light.

4 Conclusions

In this study, a technique was proposed for studying pressure sore generation, based on numeri-

cal analysis of the color content of captured images. Analysis of wounds has previously been carried out by monitoring changes in wound color. Our approach was more specifically established to study the changes in tissue color through a method which is invariant to monotonic changes in tissue color in an uncontrolled surrounding light. Small variations in the light conditions during image acquisition can affect the final decision on the state of tissue, being monitored for the assessment of pressure sores. This is because superficial signs of pressure sores initiate as small changes in the color content of the superficial layers of suspicious areas. Therefore, a quantitative technique which is invariant to small changes in the environmental light, and yet is able to distinguish these changes in tissue color, may be helpful for monitoring tissue status. It was demonstrated that the proposed technique can be used to discriminate intact tissue from slightly and considerably damaged tissues.

In this paper we dealt with artificially-induced sores which were generated in the controlled environment of the laboratory. We controlled and took into account factors such as temperature, moisture and delivered food, which could affect tissue conditions. It remains to be seen how these results will translate to patient studies, where there may be other factors affecting tissue conditions.

Acknowledgements

We would like to thank Drs. Afsar HADDADIAN and Parvin MANSOORI for assistance in data analysis.

This research has been supported with the resources and use of facilities at Tarbiat Modares University, Tehran, Iran.

References

Ahonen, T., Hadid, A., Pietikainen, M., 2006. Face description with local binary patterns: application to face recognition. *IEEE Trans. Pattern Anal. Mach. Intell.*, **28**(12):2037-2041. [doi:10.1109/TPAMI.2006.244]

Armanfard, A., Komeili, M., Kabir, E., 2008. TED: a Texture-Edge Descriptor Based on LBP for Pedestrian Detection. IEEE Int. Symp. on Telecommunications, p.643-648. [doi:10.1109/ISTEL.2008.4651380]

Bader, D., Bouten, C., Colin, D., Oomens, C., 2005. Pressure Ulcer Research: Current and Future Perspectives. Springer Verlag, London, p.1-7. [doi:10.1007/3-540-28804-X]

Belem, B., 2004. Non-invasive Wound Assessment by Image Analysis. PhD Thesis, University of Glamorgan, UK.

Berriss, W.P., Sangwine, S.J., 1997. A Colour Histogram Clustering Technique for Tissue Analysis of Healing Skin Wounds. Proc. 6th Int. Conf. on Image Processing and Its Applications, p.693-697. [doi:10.1049/cp:19970984]

Bianco, S., Gasparini, F., Russo, A., Schettini, R., 2007. A new method for RGB to XYZ transformation based on pattern search optimization. *IEEE Trans. Consum. Electron.*, **53**(3):1020-1028. [doi:10.1109/TCE.2007.4341581]

Bon, F.X., Briand, E., Guichard, S., Couturaud, B., Revol, M., Servant, J.M., Dubertret, L., 2000. Quantitative and kinetic evolution of wound healing image analysis. *IEEE Trans. Med. Imag.*, **19**(7):767-772. [doi:10.1109/42.875206]

Brown, M., Gogia, P.P., Sinacore, D.R., Menton, D.N., 1995. High-voltage galvanic stimulation on wound healing in guinea pigs: longer-term effects. *Arch. Phys. Med. Rehabil.*, **76**(12):1134-1137. [doi:10.1016/S0003-9993(95)80122-7]

Daniel, R.K., Priest, D.L., Wheatley, D.C., 1981. Etiologic factors in pressure sores: an experimental model. *Arch. Phys. Med. Rehabil.*, **62**:492-498.

Diao, C.Y., Lu, D.M., Liu, G., 2005. Relighting multiple color textures. *J. Zhejiang Univ. Sci.*, **6A**(11):1284-1289. [doi:10.1631/jzus.2005.A1284]

Galushka, M., Zheng, H., Patterson, D., Bradley, L., 2005. Case-Based Tissue Classification for Monitoring Leg Ulcer Healing. Proc. 18th IEEE Symp. on Computer-Based Medical Systems, p.353-358. [doi:10.1109/CBMS.2005.39]

Hansen, G.L., Sparrow, E.M., Kokate, J.Y., Leland, K.J., Iaizzo, P.A., 1997. Wound status evaluation using color image processing. *IEEE Trans. Med. Imag.*, **16**(1):78-86. [doi:10.1109/42.552057]

Haralick, R.M., Shanmugan, K., Dinsten, I., 1973. Textural features for image classification. *IEEE Tran. Syst. Man Cybern.*, **3**(6):610-621. [doi:10.1109/TSMC.1973.4309314]

Heikkila, M., Pietikainen, M., 2006. A texture-based method for modeling the background and detecting moving objects. *IEEE Trans. Pattern Anal. Mach. Intell.*, **28**(4):657-662. [doi:10.1109/TPAMI.2006.68]

Herbin, M., Bon, F.X., Venot, A., Jeanlouis, F., Dubertret, M.L., Dubertret, L., Strauch, G., 1993. Assessment of healing kinetics through true color image processing. *IEEE Trans. Med. Imag.*, **12**(1):39-43. [doi:10.1109/42.222664]

Jones, B.F., Plassmann, P., 1995. An instrument to measure the dimensions of skin wounds. *IEEE Trans. Biomed. Eng.*, **42**(5):464-470. [doi:10.1109/10.376150]

Kolesnik, M., Fexa, A., 2005. Multi-dimensional color histograms for segmentation of wounds in images. *LNCS*, **3656**:1014-1022. [doi:10.1007/11559573_123]

Lee, S.H., Choi, J.S., 2008. Design and implementation of color correction system for images captured by digital camera. *IEEE Trans. Consum. Electron.*, **54**(2):268-276. [doi:10.1109/TCE.2008.4560085]

Mackiewicz, M., Berens, J., Fisher, M., 2008. Wireless capsule endoscopy color video segmentation. *IEEE Trans. Med. Imag.*, **27**(12):1769-1781. [doi:10.1109/TMI.2008.926061]

Malian, A., Azizi, A., van den Heuvel, F.A., Zolfaghari, M., 2005. Development of a robust photogrammetric metrology system for monitoring the healing of bedsores. *Photogr. Rec.*, **20**(111):241-273. [doi:10.1111/j.1477-9730.2005.00319.x]

Nischik, M., Forster, C., 1997. Analysis of skin erythema using true color images. *IEEE Trans. Med. Imag.*, **16**(6):711-715. [doi:10.1109/42.650868]

Oduncu, H., Hoppe, A., Clark, M., Williams, R.J., Harding, K.J., 2004. Analysis of skin wound images using digital color image processing: a preliminary communication. *Int. J. Lower Extrem. Wounds*, **3**(3):151-156. [doi:10.1177/1534734604268842]

Ojala, T., Pietäikinen, M., Harwood, D., 1996. A comparative study of texture measures with classification based on feature distributions. *Pattern Recogn.*, **29**(1):51-59. [doi:10.1016/0031-3203(95)00067-4]

Perez, A.A., Gonzaga, A., Alves, J.M., 2001. Segmentation and Analysis of Leg Ulcers Color Images. Proc. Int. Workshop on Medical Imaging and Augmented Reality, p.262-266. [doi:10.1109/MIAR.2001.930300]

Plassmann, P., Jones, T.D., 1998. MAVIS: a non-invasive instrument to measure area and volume of wounds. *Med. Eng. Phys.*, **20**(5):332-338. [doi:10.1016/S1350-4533(98)00034-4]

Plassmann, P., Jones, B.F., Ring, E.F.J., 1995. A structured light system for measuring wounds. *Photogr. Rec.*, **15**(86):197-204. [doi:10.1111/0031-868X.00025]

Salcido, R., Fisher, S.B., Donofrio, J.C., Bieschke, M., Knapp, C., Liang, R., LeGrand, E.K., Carney, J.M., 1995. An animal model and computer controlled surface pressure delivery system for the production of pressure ulcers. *J. Rehabil. Res. Dev.*, **32**(2):149-161.

Salter, R., Love, H., Fright, R., Nixon, M., 2006. PDA-based, portable laser scanner measurement of wound size: accuracy and reproducibility. *ANZ J. Surg.*, **76**(Suppl 1):A59.

Tajeripour, F., Kabir, E., Sheikhi, A., 2008. Fabric defect detection using modified local binary patterns. *EURASIP J. Adv. Signal Process.*, **2008**, Article ID 783898, p.1-12. [doi:10.1155/2008/783898]

Theodoridis, S., Koutroumbas, K., 2003. Pattern Recognition (2nd Ed.). Academic Press, London, p.270-272.

Torkaman, G., Sharafi, A.A., Fallah, A., Katoozian, H.R., 2000. Biomechanical and Histological Studies of Experimental Pressure Sores in Guinea Pigs. Proc. 10th Int. Conf. on Biomedical Engineering, p.463-469.

Treuillet, S., Albouy, B., Lucas, Y., 2009. Three-dimensional assessment of skin wounds using a standard digital camera. *IEEE Trans. Med. Imag.*, **28**(5):752-762. [doi:10.1109/TMI.2008.2012025]

Zheng, H., Bradley, L., Patterson, D., Galushka, M., Winder, J., 2004. New Protocol for Leg Ulcer Classification from Colour Images. Proc. IEEE 26th Annual Int. Conf. on Engineering in Medicine and Biology Society, p.1389-1392. [doi:10.1109/IEMBS.2004.1403432]